Available online at www.sciencedirect.com
SCIENCE DIRECT®
Journal of Power Sources 124 (2003) 403–414
JOURNAL OF POWER SOURCES
www.elsevier.com/locate/jpowsour

Visualization of water buildup in the cathode of a transparent PEM fuel cell

Klaus Tüber*, David Pócza, Christopher Hebling

Fraunhofer Institute for Solar Energy Systems ISE, Heidenhofstrasse 2, D-79110 Freiburg, Germany

Received 27 January 2003; received in revised form 26 June 2003; accepted 30 June 2003

Abstract

Two-phase flow and transport of reactants and products in the cathode of a transparent proton exchange membrane fuel cell (PEMFC) are studied experimentally. Images of water formed inside the cathode gas channels are presented to explain the phenomenon of water flooding. Effects of air stoichiometry, temperature, air humidity and different characteristics of diffusion layers are discussed. The influence of hydrophobic and hydrophilic diffusion layers compared to standard carbon papers on water transport is investigated. Mathematical verification of a threshold current density corresponding to first appearance of liquid water at the membrane/cathode interface confirms the experimental results.

Keywords: PEMFC; Two-phase flow; Water transport; Cathode flooding; Diffusion layer; Mathematical model

1. Introduction

High efficiencies, low emissions and the modular designs of proton exchange membrane fuel cells (PEMFCs) have made them an attractive power source for stationary co-generation units, automotive applications as well as for portable applications to complement and substitute batteries of consumer electronics (e.g. laptop computers and mobile phones) and industrial electrical loads (e.g. autonomous sensors) [1,2]. In a PEMFC, hydrogen and oxygen react electrochemically to water, producing electricity and heat. Several coupled fluid flow, heat and mass transfer processes occur which have a significant impact on thermal and water management and mass transport limitations. While thermal management is required to remove the heat in order to prevent dehydration of the membrane and excessive operating temperatures, proper water management ensures that the membrane remains fully hydrated and therefore maintains good ionic conductivity and performance. Mass transfer limitations are associated with gas diffusion processes in the diffusion layers and the porous electrodes. Above a certain current density, they can result in starvation of the reactants, generally oxygen.

The present paper focuses on the important issue of cathode flooding in small fuel cells for portable applications operated at ambient conditions. Constant voltage discharge performance of a transparent PEMFC running on dry hydrogen is compared with pictures taken with a digital camera during operation. These images of the internal cathode flow field visualize the formation of water. It is shown that not only the pores of the gas diffusion layer but also total air channels are filled with liquid water blocking the transport of reactants to the reaction sites. Simultaneously appearing performance losses make the relevance of a capable water management clear. The experimental results are compared to analytical models that describe single- and two-phase transport regimes.

2. Water management and transport

The problem of water management and transport in PEM fuel cells has been the subject of several experimental [3–7] and theoretical [8–18] studies. The main parts of a PEMFC are the membrane electrode assembly (MEA), diffusion layers to homogeneously distribute fuel and oxidizer, and bipolar plates with machined groves that provide flow channels. The proton conductivity of the polymer electrolyte membrane is highly dependent on the water content of the membrane. If there is not enough water, the polymer dries out and its resistance to proton conduction increases

* Corresponding author. Tel.: +49-761-4588-5207; fax: +49-761-4588-9207.
E-mail address: ktueber@ise.fhg.de (K. Tüber).

0378-7753/$ – see front matter © 2003 Elsevier B.V. All rights reserved.
doi:10.1016/S0378-7753(03)00797-3

Nomenclature

D	diffusivity
F	Faraday constant
h_m	interfacial mass transfer coefficient
H	height
I_{cr}	critical or threshold current density
L	length of cathode channel
$\dot{m}$	mass flow
M	molecular weight
P	operating pressure
P_e	electrical output power
R	gas constant
RH	relative humidity
T	gas temperature
u	velocity
V_c	mean voltage of each cell in a fuel cell stack

Greek letters

α	net water transport coefficient per proton
ε	effective porosity of gas diffusion cathode
λ	air stoichiometry
ν	diffusion volume
ρ	density
ϖ	water ratio

Superscripts

B	component
g	gaseous
H_2O	water
l	liquid
O_2	oxygen

Subscripts

ac	air channel
air	air-flow
A	component
c	cathode
in	gas inlet
out	gas outlet
prod	product
sat	saturated water vapor

dramatically resulting in a performance loss [7,19]. As described in [5,7,13,16], the water balance is affected by different mechanisms that are sketched in Fig. 1.

Water may be supplied by humidified reactants or by direct liquid hydration [20,21]. During operation, water tends to migrate from the anode to the cathode by protons moving through the electrolyte under the electro-osmotic drag [16,22]. Since water is formed in the electrochemical reaction at the cathode, water concentration on the cathode side is usually higher than on the anode side. A back diffusion of water from cathode to anode follows caused by the increasing gradient of water concentration in the membrane [3,7]. This effect can be intensified by hydraulic permeation due to higher gas pressure on the cathode side than on the anode side [23]. Altogether, these transport mechanisms can lead to a water movement from the electrodes into the gas channels, where the gaseous and/or liquid water will be removed by hydrogen and air, respectively leaving the fuel cell. If the water generated is not removed from the electrode at a sufficient rate, flooding may result and the transport of reactants is hindered [9]. In our experiments this is especially evident in the cathode of fuel cells when operated at ambient pressure and low temperatures (<30 °C) as they occur during startup and outdoor operation.

3. Experimental

3.1. Design of the transparent PEM fuel cell

To investigate water buildup in a PEMFC, a transparent design similar to the one presented in [24] is required. Fig. 2 describes a schematic top and side view of the transparent fuel cell used in our research. In order to allow a clear distinction between cause and effect concerning the cell performance, the design is consciously simple.

Basically, our PEMFC consists of a Gore PRIMEA® membrane–electrode assembly (Series 5510, ionomer thickness between electrodes: 35 μm, catalyst loading of anode and cathode: 0.3 mg Pt/cm^2) sandwiched between standard TORAY® carbon paper (TGP-H-090). This set-up is placed between a base and a transparent cover plate. While the anodic base plate is fabricated of stainless steel, the cover plate is made of plexiglass. To obtain the necessary electric connection, a rib of stainless steel is inserted into a slot in the cover plate. A copper wire realizes the contact between an electrical load and the fuel cell. Due to the design of rib and slot, two air channels are formed with a channel width of 1.5 mm, a depth of 1 mm and a length of 50 mm. The air is directed from the inlet tube on the left to the outlet tube on the right. The flow field on the anode side is constructed similarly to the cathode flow field. The active area of 62 mm × 6.5 mm of the fuel cell is defined by the gasket. Both plates are fixed with eight M4 screw joints tightened with a torque of 1 Nm. This results in a high reproducibility of clamping pressure that directly influences the electrical contact resistance [25].

3.2. Experimental set-up

The experimental set-up shown in Fig. 3 consists of a gas supply unit, the fuel cell to be investigated, a digital camera, an electrical load, different sensors, a data-acquisition system and a computer for analysis.

The reactants air and hydrogen are regulated by mass flow controllers (Type 1179, MKS). While the air can be humidified in a range of 10–100% RH at ambient temperatures, the

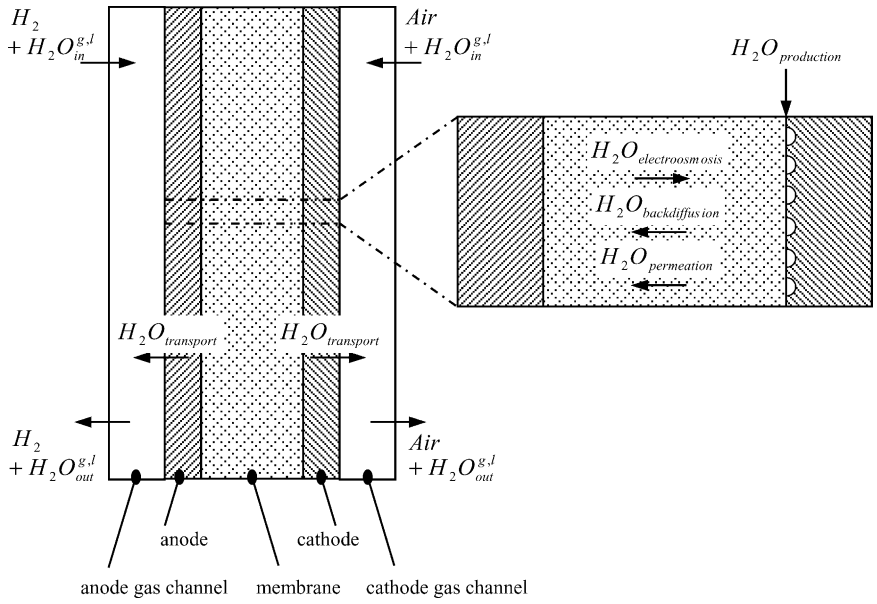

Fig. 1. Scheme of water movement in a PEMFC. The direction of water transport may be reversed, due to operation conditions.

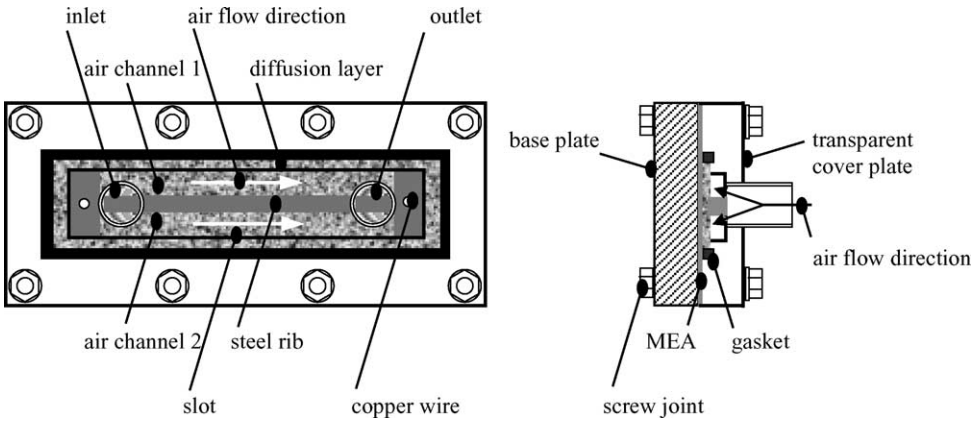

Fig. 2. Schematic top and side view of the transparent PEMFC.

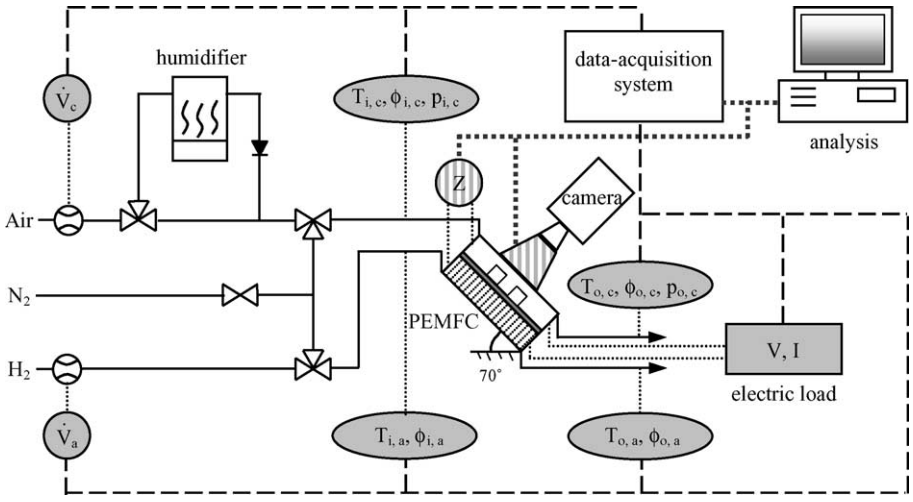

Fig. 3. Experimental set-up.

hydrogen is delivered dry. It is possible to purge the electrodes with nitrogen between two measurements to realize reproducible initial conditions. The temperature and relative humidity of the reactants are recorded at inlet and outlet by small thermocouples and industrial transmitters (I-155C, Rotronic). Furthermore, the pressure difference (Type DPS, FSM) between inlet and outlet of cathode is quantified. The fuel cell is connected to an electric load (HP88-20, Bank) that is operated in a constant voltage discharge mode. All physical parameters like current and voltage of the fuel cell, gas volume flow of the reactants, pressure drop in the cathode flow field, relative humidity and temperatures of air and hydrogen are recorded with the data-acquisition system (34970A, Agilent). Electric impedance measured with a milliohmmeter at 1 kHz (4328 A, HP) and photos taken during operation with a digital camera complete the data set. Due to an optimized adjustment of the digital camera the PEMFC is positioned 70° to the horizontal.

3.3. Experimental conditions

Results presented in the following section are performed in a constant voltage discharge mode (500 mV) for 40 min at ambient pressure. While hydrogen is fed dry (<10% RH) to the anode at a constant flow rate of 35 ml/min, the air humidity is adjusted to 60% RH. Thereby, the air-flow rate varies within different experiments. Inlet temperatures of both gases are around 23 °C and the fuel cell is not tempered. The absolute value of impedance can decrease slightly during operation due to increasing water content of the membrane. To achieve reproducible conditions, the impedance is adjusted to approximately 130 mΩ by drying the membrane with nitrogen before each experiment.

4. Results and discussion

4.1. Water buildup observed during constant voltage discharge mode

Fig. 4 characteristically describes the current density as a function of operating time during the constant voltage (500 mV) discharge mode of the transparent fuel cell. The

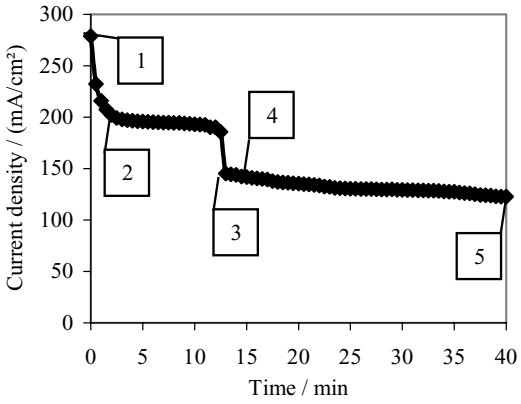

Fig. 4. Constant voltage (500 mV) discharge performance.

air-flow rate is adjusted to 150 ml/min. The numbers (1–5) indicate the time when photos were taken.

At the beginning of each measurement, the fuel cell is loaded from open circuit voltage down to the constant voltage of 500 mV. The corresponding current density is 278 mA/cm^2. In the following 3 min this value decreases substantially down to 198 mA/cm^2. This effect is ascribed to "partial flooding" of the cathode catalyst layer. As described in [13,26] this can lead to a reduction of the effective porosity. The photos presented in Fig. 5 show that not only the electrode is flooded but also the cathode diffusion layer.

Photo 1 is taken while the reactants are applied and the fuel cell is operated in open circuit mode. A condensation of water cannot be observed and channel 1 and 2 are water free. Photo 2 is taken after 3 min of operation. It shows areas of the carbon paper that have changed color near the air inlet on the left and near the outlet on the right. Here, the product water migrates into and through the diffusion layer and becomes visible as dark spots. Additionally, water vapor is appearing close to the inlet. As the enlarged picture shows, this vapor can condense at the cover plate in the form of very small droplets. The fact that water occurs near inlet and outlet is attributed to the resulting air-flow conditions. While the gas transport in the channels is convective, it is diffusive in the areas under the rib. Here, the air volume flow is much lower than in the channels and the gas can hardly remove product water. The concentration of water increases and water can

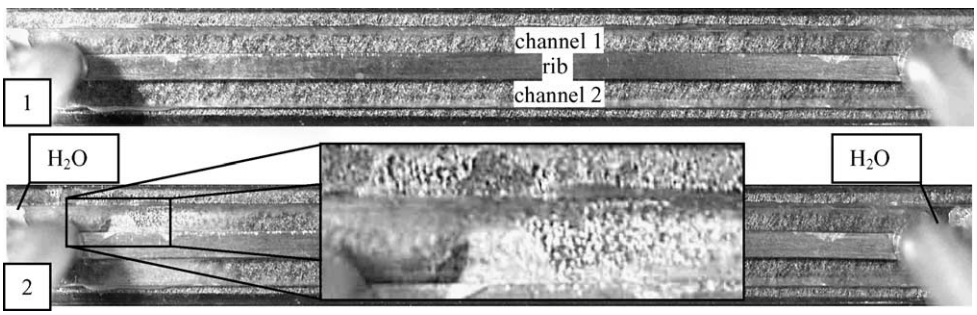

Fig. 5. Photos taken before discharging (1) and after 3 min (2) of operation.

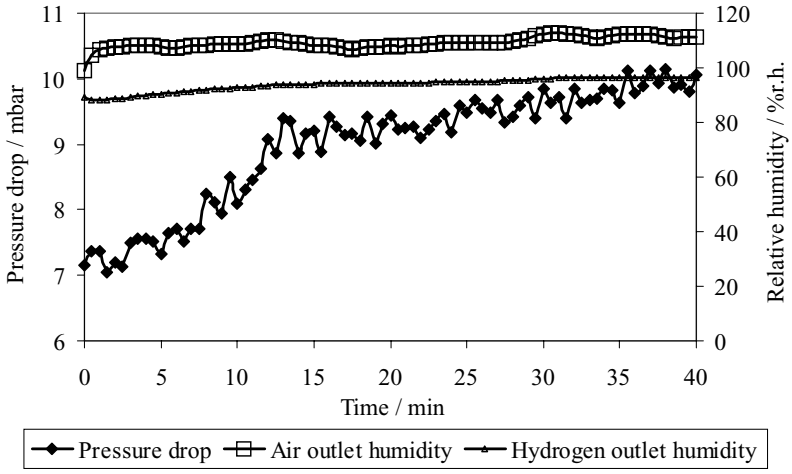

Fig. 6. Reactant outlet humidity and cathode pressure drop during operation.

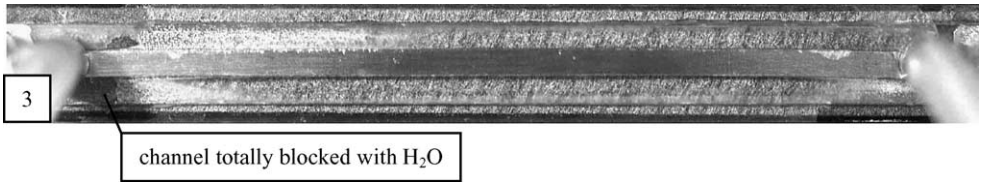

Fig. 7. Photo taken after 13 min (3) of operation.

penetrate through the cathode diffusion layer. The fact that enough water is produced to partially flood the carbon paper is verified by the outlet humidity of the reactants and the pressure drop in the cathode flow field, see Fig. 6.

The humidity characteristics of both gases show that even at the beginning of the operation, outlet humidities of around 100% RH are reached. The detection limit of the humidity sensors is immediately exceeded and it can be assumed that hydrogen and air are oversaturated. During further operation, the gas humidities show no significant change. Both gases remain saturated and even a partial flooding of the anode could occur. At ambient temperatures of around 23 °C, the exhaust temperatures of hydrogen and air are measured to be approximately 26.5 °C. Possible reasons for such a marginal warming up are low heat generation due to the low current densities and cooling effects caused by forced convection of relatively high gas volume flows.

Another indication of electrode flooding is the increase of the pressure drop along the channel. It rises from 7.15 mbar at the beginning of the experiment up to 9.4 mbar after 13 min. This is an increase of more than 30%. The water produced reduces the cross-section of the gas channels and total clogging of an air channel can result, as presented in Fig. 7.

Next to the water already observed after 3 min (see Fig. 5), additional water has accumulated near the inlet and outlet, which lead to a complete blockage of the lower channel 2. The air-flow in channel 2 is interrupted and an enormous decline of current density can be observed in Fig. 4. Current density falls from 185 down to 145 mA/cm^2. This collapse is followed by a marginal decrease of current density, which can be described with Fig. 8.

Between 13 and 40 min of operation, a further water accumulation can be observed. More and more channel vol-

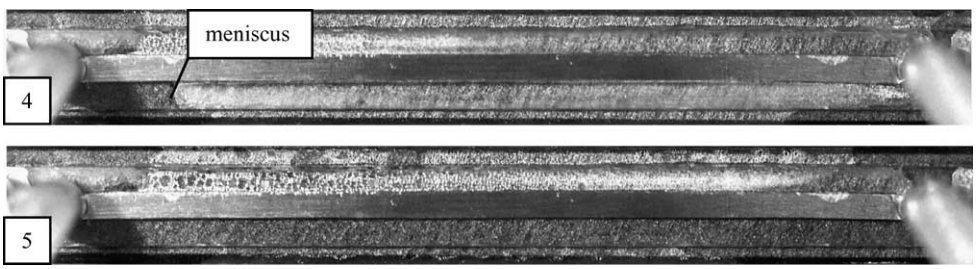

Fig. 8. Photos taken after 15 min (4) and at the end (5) of operation.

ume is filled with water and the arising meniscuses move from inlet to outlet and vice versa. At the end of the measurement, the entire channel 2 is filled with product water. Although condensation of water droplets increases near the gas inlet and small amount of water is buildup near the outlet, channel 1 remains open due to the forced convection of air. The fact that the current density decreases only slightly during the last 27 min points out that in the first few minutes of operation the cathode is already flooded. The water becoming more and more visible is pushed from the catalyst layer through the diffusion layer into the channel. However, the performance loss mainly depends on the flooding of the cathode. In the following, different possibilities of influencing the electrode flooding are discussed and analytical models and further experiments are compared.

4.2. Effect of air stoichiometry

Air-flow is generally used for water removal. Usually, the air stoichiometry is at least "2" to minimize concentration losses [27]. If the cathode should be prevented from flooding, the product water must be evaporated by the air-flow. The maximum effect of drying is reached when the air is saturated. This state is achieved when the saturated vapor pressure of water $p_{\mathrm{sat}}^{\mathrm{H_2O}}$ is equal to the partial pressure of water at the air outlet $p_{\mathrm{air,out}}^{\mathrm{H_2O}}$:

$$p_{\mathrm{sat}}^{\mathrm{H_2O}} = p_{\mathrm{air,out}}^{\mathrm{H_2O}} \tag{1}$$

The saturated vapor pressure of water in bar can be expressed as a function of temperature (°C) [16]:

$$p_{\mathrm{sat}}^{\mathrm{H_2O}} = 10^{-2.174+0.02953T-9.1837\cdot10^{-5}T^2+1.4454.10T^3} \tag{2}$$

Assuming that the total amount of product water is evaporated and that water vapor and air are behaving like perfect gases, the partial pressure of water at the air outlet is defined as follows [27]:

$$p_{\mathrm{air,out}}^{\mathrm{H_2O}} = \frac{\varpi_{\mathrm{air,out}}\, p}{\varpi_{\mathrm{air,out}} + 0.622} \tag{3}$$

The water ratio $\varpi_{\mathrm{air,out}}$ can be calculated from the fraction of the mass flows in ml/min of water $\dot{m}_{\mathrm{air,out}}^{\mathrm{H_2O}}$ contained in the outlet air and of dry air at the outlet $\dot{m}_{\mathrm{air,out}}$:

$$\varpi_{\mathrm{air,out}} = \frac{\dot{m}_{\mathrm{air,out}}^{\mathrm{H_2O}}}{\dot{m}_{\mathrm{air,out}}} = \frac{\dot{m}_{\mathrm{prod}}^{\mathrm{H_2O}} + \dot{m}_{\mathrm{air,in}}^{\mathrm{H_2O}}}{\dot{m}_{\mathrm{air,out}}} \tag{4}$$

Other than the considerations presented in [27], the mass flow of water in the outlet air is a combination of product water flow $\dot{m}_{\mathrm{prod}}^{\mathrm{H_2O}}$ and the water content of the input air-flow $\dot{m}_{\mathrm{air,in}}^{\mathrm{H_2O}}$. If water transport from anode to cathode and vice versa is ignored, the water flow produced and the water flow of the cathode outlet can be expressed as follows [27]:

$$\dot{m}_{\mathrm{prod}}^{\mathrm{H_2O}} = 9.34 \times 10^{-8} \frac{P_{\mathrm{e}}}{V_{\mathrm{c}}} \tag{5}$$

$$\dot{m}_{\mathrm{air,out}} = (3.57 \times 10^{-7}\,\lambda - 8.29 \times 10^{-8}) \frac{P_{\mathrm{e}}}{V_{\mathrm{c}}} \tag{6}$$

where P_{e} is the electrical output power (W), V_{c} the mean voltage of each cell in a fuel cell stack (V) and λ the air stoichiometry.

The mass flow of water in the inlet air can be calculated as a product of water ratio and air-flow at the inlet. The water ratio is expressed for an ideal gas–vapor mixture as presented in [28] and the air usage is quantified as in [27]:

$$\dot{m}_{\mathrm{air,in}}^{\mathrm{H_2O}} = \varpi_{\mathrm{air,in}} \dot{m}_{\mathrm{air,in}} = \left(0.622 \frac{p_{\mathrm{sat}}^{\mathrm{H_2O}}}{p/\mathrm{RH}_{\mathrm{air,in}} - p_{\mathrm{sat}}^{\mathrm{H_2O}}}\right) \times \left(3.57 \times 10^{-7}\,\lambda \frac{P_{\mathrm{e}}}{V_{\mathrm{c}}}\right) \tag{7}$$

The combination of Eqs. (1)–(7) can be solved analytically. The results are visualized in form of a temperature versus air stoichiometry characteristic, see Fig. 9.

Fig. 9 presents the dependence of stoichiometry needed to reach saturated water vapor at air outlet subject to temperature (0–100 °C) and inlet humidity (30, 60 and 90% RH) of air. If the air stoichiometry is lower than the curves predict, the cathode tends to flood. If the stoichiometry were higher, the humidity of the outlet air would be lower than 100% RH. It can be seen, that, e.g. for air with a relative humidity of 60% RH and a stoichiometry of 2, the air temperature of about 73 °C should not be exceeded. Otherwise, the air is not fully humidified and the cathode tends to dehydrate over the total active area. Therefore, reactants of PEM fuel cells operating at temperatures of more than 60 °C are humidified [3,27]. The opposite consideration can be made for PEM fuel cells operating at room temperature, e.g. 20 °C. In the case of 60% RH an air stoichiometry of more than 43 has to be supplied to avoid liquid water. Here, limiting factors of pumps and compressors are reached. It has to be emphasized that the drying effect of water, or the rate of evaporation of water, is directly proportional to the difference between the water partial pressure and the saturated

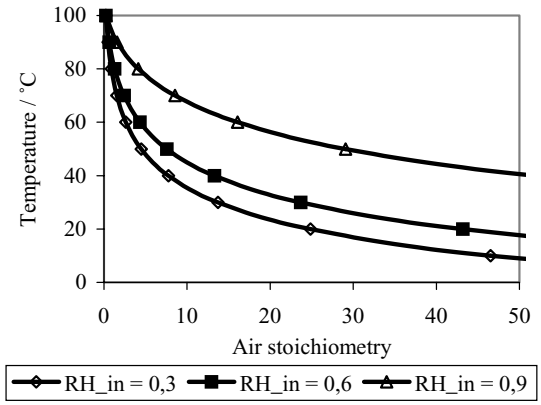

Fig. 9. Stoichiometry needed to obtain fully humidified outlet air depending on temperature and inlet humidity.

vapor pressure. Non-linear variation of the saturated vapor pressure with temperature Eq. (2) makes high demands on water management technologies.

Similar results can be obtained with another analytical estimation presented in [8]. Here, the onset of two-phase operating regime is defined by a corresponding threshold current density that identifies first appearance of liquid water in the vicinity of the membrane/cathode interface:

$$I_{cr} = \frac{2F}{M^{H_2O}} \frac{\rho_{sat}^{H_2O}(1 - RH_{air,in})}{1 + 2\alpha} \times \left(\frac{L}{H_{ac}} \frac{1}{u_{air,in}} + \frac{1}{h_m} + \frac{H_c}{\varepsilon D_{air}^{H_2O}} \right)^{-1} \quad (8)$$

The critical current density in mA/cm^2 is depending on the water vapor diffusion resistance in the porous cathode, the mass transfer resistance at the porous cathode/air channel interface, and the ability of air to evaporate water. It reduces with the increases of the relative humidity at the gas inlet, channel length and porous cathode thickness and the decreases of inlet velocity, operating temperature and channel height. The different parameters and operating conditions to calculate the effect of air inlet velocity corresponding to air inlet flow rate on the threshold current density of our fuel cell are listed in Table 1.

The density of saturated water vapor $\rho_{sat}^{H_2O}$ is calculated for a gas temperature of 25 °C by Eq. (2). The parameter α that represents the net water molecule per proton flux ratio is affected by electro-osmotic drag by electric field, fluid convection by pressure difference, and molecular diffusion by species concentration difference in the membrane region. Among other things, the net water transfer coefficient is dependent on thickness and water content of the membrane, current density and position along the gas channels. It must be considered that positive as well as negative values are reported [5,14,15,17,30]. In our case of using ultra-thin membranes and operating the PEMFC at a very low current density an average net water transfer coefficient α of −0.2 is assumed. This means that the hydrogen gas stream will be humidified by water dragging from cathode to anode, which is verified by our experimental data. Wang et al. [8] have shown that the mass transfer coefficient between porous cathode and air channel h_m can be calculated by

$$h_m = \frac{2.693 D_{air}^{O_2}}{H_{ac}} \quad (9)$$

Thereby, the binary diffusion coefficient D_A^B of a gas mixture in cm^2/s can be calculated as presented in [29]:

$$D_A^B = \frac{1.013 \times 10^{-3}(T + 273.15)^{1.75}}{p(\nu_A^{1/3} + \nu_B^{1/3})^2} \sqrt{\frac{M_A + M_B}{M_A M_B}} \quad (10)$$

where T is the gas temperature in °C, p the pressure in bar, ν the diffusion volume of components A and B [29], and M the molecular weight of components A and B in kg/kmol.

The cathode height H_c is a combination of the diffusion layer and cathode catalyst thickness. While the thickness of an uncompressed TGP-H-090 is about 280 μm [31], the cathode catalyst layer is assumed to be 10 μm. The total height H_c of the compressed cathode is assumed to be 230 μm. Like the cathode thickness, the effective porosity of the carbon paper is affected by compression. It is assumed that the porosity ε reduces from 0.78 [31] down to 0.5 for a compressed and possibly water flooded TGP-H-090. Using the presented parameters, the calculation of the threshold current density subject to the inlet velocity of air $u_{air,in}$ in cm/s is realized and illustrated in Fig. 10.

In Fig. 10 it can be seen that the threshold current density I_{cr} approaches an asymptotic value of 220 mA/cm^2 at an air-flow rate of about 1000 ml/min. The curve divides the parameter zone into single- and two-phase flow. Below the

Table 1
Parameters and operating conditions used for calculating the critical current density depending on air inlet velocity $u_{air,in}$

Parameter	Symbol	Value	Source
Faraday constant	F	96,487 °C/mol	[8]
Molecular weight of water	M^{H_2O}	0.18015 kg/mol	[28]
Density of saturated water vapor	$\rho_{sat}^{H_2O}$	1.391×10^{-8} kg/cm^3	(Eq. (2)), calculated
Relative humidity at the air inlet	$RH_{air,in}$	60% RH	
Gas temperature	T	25 °C	Averaged
Gas constant	R	8.315 J/(mol K)	[28]
Net water transport coefficient per proton	α	−0.2	Assumed
Length of cathode channel	L	5 cm	
Air channel height	H_{ac}	0.1 cm	
Interfacial mass transfer coefficient	h_m	5.395 cm/s	(Eq. (9)), calculated
Oxygen diffusivity	$D_{air}^{O_2}$	0.2 cm^2/s	(Eq. (10)), calculated
Operating pressure	P	1 bar	
Cathode height (=diffusion layer + cathode)	H_c	0.023 cm	Assumed
Effective porosity of gas diffusion cathode	ε	0.5	Assumed
Water vapor diffusivity	$D_{air}^{H_2O}$	0.255 cm^2/s	(Eq. (10)), calculated

Most of the parameters are physical constants, geometrical dimensions of the transparent PEM fuel cell and operating conditions. Others have to be calculated and assumed.

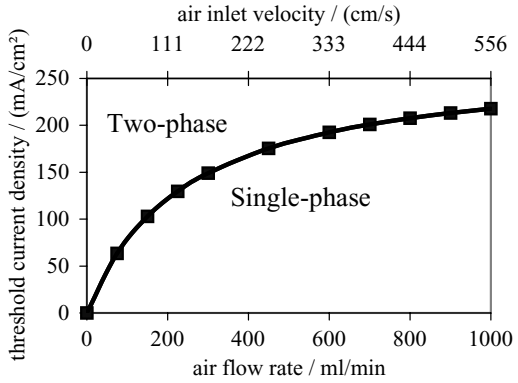

Fig. 10. Effect of flow rate and inlet velocity of air, respectively, on the threshold current density.

critical current density single-phase flow is specified, above I_{cr} two-phase flow appears. Under this condition, the water vapor removal is limited by diffusion through the porous cathode.

To verify the analytical models presented above, experimental measurements are performed with different air-flows. The results of current density characteristics at constant voltage (500 mV) discharge mode versus operating time are presented in Fig. 11.

In all three cases (150, 225 and 450 ml/min air-flow), a substantial decrease of current density can be observed during the first few minutes. The current densities fall from around 250 down to approximately 200 mA/cm^2. It seems that partial flooding of the electrodes cannot be prevented. A possible reason for such an effect can be seen in the surface temperatures of these PEMFC components that are lower than the temperature of steam. Especially, in the beginning of a test run when the cell temperature is low, condensation may occur.

In case of air-flow rates of 150 and 225 ml/min a second sharp decline appears. As presented in Section 4.1, channel flooding that interrupts the air supply for channel 2 causes this drop. Due to higher gas flow rates, more water

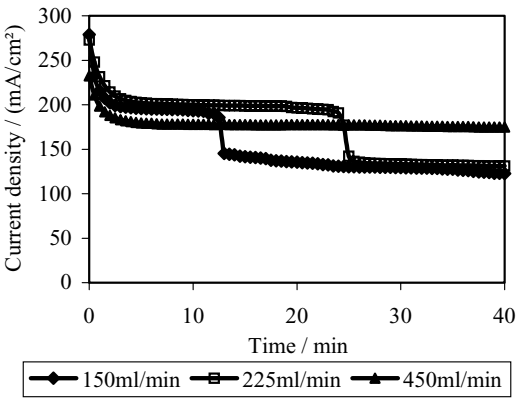

Fig. 11. Constant voltage (500 mV) discharge mode depending on different air-flows.

can be evaporated and the slump in case of 225 ml/min occurs 12 min later than in case of 150 ml/min. Opposite to these characteristics, the current density curve for air-flow of 450 ml/min does not show a second drop. The stoichiometry is high enough to lead away the product water in gaseous form. The current density remains steady at a level of 175 mA/cm^2 and liquid water cannot be observed in the cathode flow field. Furthermore, the gas humidities at the outlets stay below 100% RH. While hydrogen outlet humidity is measured to be less than 75% RH, the humidity of air at the outlet remains below 92% RH. The gas outlet temperatures are in the range of 26.5 °C.

To compare the experimental results with the first analytical model the air-flow rates have to be converted into stoichiometry. Due to unsteady run of current density the calculation of stoichiometry factors is realized with the average current density. From this follows a stoichiometry of 12, 17 and 38 for the different air-flow rates 150, 225 and 450 ml/min and associated average current densities of 193, 200 and 178 mA/cm^2, respectively. Comparing the experimental data with Fig. 9, it can be seen that for a temperature of 26.5 °C and an inlet humidity of 60% RH a stoichiometry of 29 is necessary to reach fully humidified air at the outlet. In the cases of air-flow rates of 150 ml/min and 225 ml/min, this value is not reached and liquid water blocks one air channel after a certain time. In case of a stoichiometry of 38, the limiting stoichiometry of 29 is exceeded and flooding can be prevented. The gas humidity remains below 100% RH, which is a reference for single-phase transport. The experimental results agree with the analytical model that is displayed in Fig. 9.

Comparing the calculated critical current density with the quasi-stationary current density reached after 40 min of operation at a flow rate of 450 ml/min, presented in Fig. 11, fundamental correspondence can be verified. The threshold current density of 175 mA/cm^2 agrees with the experimental value. Only in the first minutes of operation, the current density is higher than the critical current density. Corresponding two-phase flow results in a decrease of porosity of the carbon paper due to liquid water. This effect justifies the assumption of reducing the porosity of the carbon paper. In the further run of the experiment, the current density remains below the threshold current density of 175 mA/cm^2. Therefore, a two-phase flow in terms of forming steam or condensate cannot be observed in the air channels.

In comparison with the experiment at a flow rate of 450 ml/min, results observed at flow rates of 225 and 150 ml/min show different behavior. Due to the fact that in case of air-flow rates of 225 and 150 ml/min the threshold current densities of 130 and 103 mA/cm^2 are widely overstepped, the air channels are blocked by occurring liquid water, compare Figs. 7 and 8. To remove the water droplet in a clogged channel, a pressure drop is necessary that leads to a driving force that is higher than the frictional force between droplet and walls. But in case of flow fields with parallel air channels the pressure drop can be very small and

water removal becomes impossible. Due to the fact that in case of small fuel cells for portable applications peripherals like tempering units, external humidifiers, pressurization and flow regulation systems are not considered because of size and auxiliary power demand, other effects to manipulate the water buildup in the flow field must be taken into consideration. Otherwise, enormous loss of electric power will be observed.

Here, passive options to manipulate the water transport in a PEMFC are investigated rather than active possibilities of intervention. In the following section, the effects of hydrophobic and hydrophilic carbon papers on the water buildup in our transparent fuel cell are studied. Again, photos of inside the air-flow field support the experimental measurements.

4.3. Effect of diffusion layer characteristic

The basically hydrophobic character of untreated carbon papers can be increased by PTFE [32–34] or decreased by a hydrophilic coating. PTFE coating that is also used to hydrophobize catalyst layers of membrane electrode assemblies [35–37] expels the product water to obtain effective gas diffusion. Hydrophilic clusters in polymer electrolyte membranes maintain water inside the MEA to guarantee sufficient proton conductivity [27]. As presented in Sections 4.1 and 4.2, the problem in case of fuel cells operated at temperatures around 30 °C is not dehydration of the MEA but flooding of gas channels. The idea to hydrophilize carbon papers is to absorb and widely distribute the product water inside the backing layer. Thereby, total clogging of gas channels as presented in Fig. 7 shall be prevented.

The process of PTFE coating is realized similar to the preparation presented in [32]. The carbon paper (TGP-H-090) is cleaned in an ultrasonic bath, and then dried for 30 min at a temperature of 60 °C. Afterwards the diffusion layer is slowly lowered into a 10% PTFE suspension where it remains for 10 min. Then the paper is dried at 60 °C for 30 min and sintered at 300 °C for 15 min. Before the diffusion layer is assembled, it is cleaned and dried once more at 60 °C for 30 min. The PTFE weight content absorbed by the hydrophobized carbon paper after the treatment is 25 wt.%. This so-called PTFE/carbon paper weight ratio is calculated as presented in [32].

Our first experiments to hydrophilize diffusion layers of PEM fuel cells are carried out with sodium dodecyl sulfate (SDS, $C_{12}H_{25}NaO_4S$). Five hundred milligrams of this surface-active tenside is solubilized in 100 ml distilled water. After cleaning the carbon paper (TGP-H-090) in an ultrasonic bath, it is dried for 30 min in an oven tempered at 60 °C. Then it is immersed for 15 min into the SDS suspension that is located in an ultrasonic bath. This enables the sodium dodecyl sulfate to distribute uniformly within the diffusion layer. In the end it is dried for 30 min at a temperature of 60 C. The SDS weight content absorbed by the hydrophilized carbon paper after the treatment is about 1 wt.%.

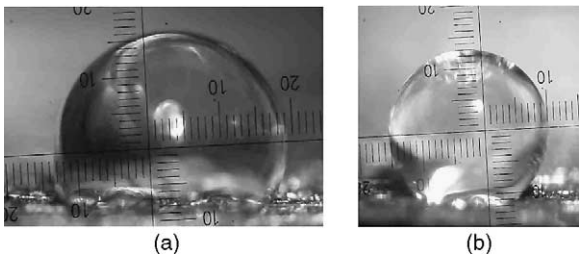

Fig. 12. Wetting behaviour of (a) standard and (b) hydrophobized TGP-H-090.

To characterize the wetting behavior of the variably treated diffusion layers, small water droplets are applied. Fig. 12 presents side views of these droplets on the carbon paper surface.

The interaction between fluid and surface can be described by the contact angle. It is obvious that this angle is greater in the case of the hydrophobized diffusion layer than in the case of the standard carbon paper. As opposed to standard and hydrophobized diffusion layers, a qualitative measurement of the contact angle for a hydrophilic carbon paper is impossible. Instead of forming discrete droplets the liquid applied to the surface is directly absorbed. Within a few microseconds, droplets of the same size than shown in Fig. 12 are widely distributed inside the porous paper over an area with a diameter of around 10 mm. The hydrophilized carbon paper acts like a sponge.

In Fig. 13, the influence of hydrophobicity and hydrophilicity of carbon paper on fuel cell performance is compared to measurements with untreated TGP-H-090. In all cases, diffusion layers on anode and cathode are likewise changed and the air-flow rate is adjusted to 225 ml/min.

As previously described, the current density decreases in all three cases due to partial flooding of the cathode. But, as can be seen from the run of curves, the reduction in case of the hydrophilic carbon paper is less sudden than in the other cases. Both characteristics of standard and

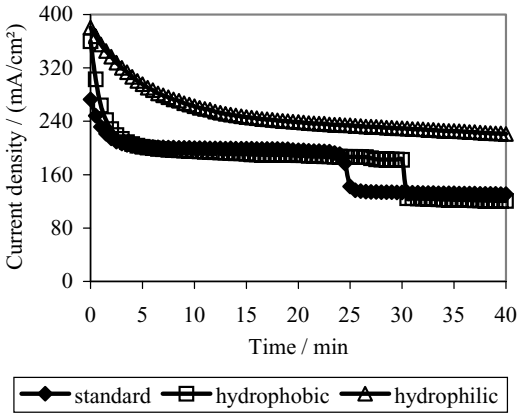

Fig. 13. Effect of carbon paper characteristic on constant voltage (500 mV) discharge performance.

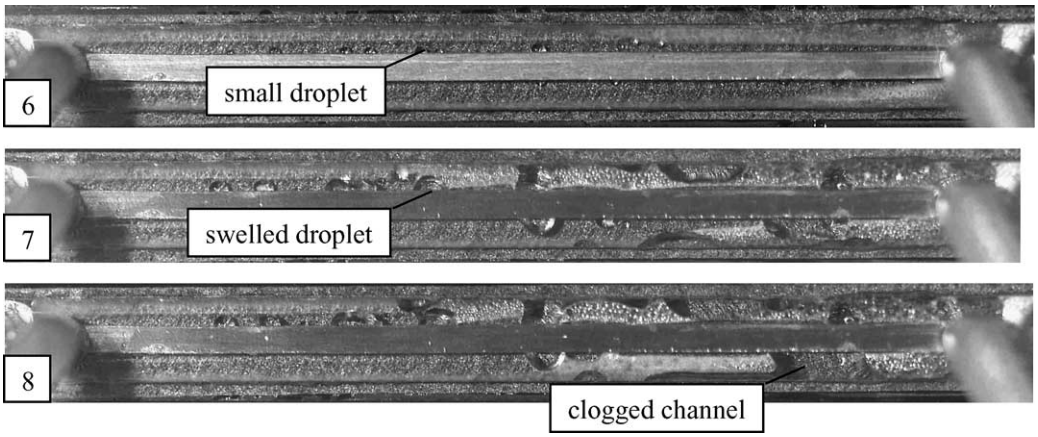

Fig. 14. Photos taken after 5 min (6), 25 min (7) and 30 min (8) of operation with a hydrophobic diffusion layer.

hydrophobic carbon paper deteriorate in the first 4 min down to about 200 mA/cm^2. This value remains almost steady in the next few minutes before a second slump occurs. In case of the standard diffusion layer current density falls down after 25 min. Five minutes later the performance drop of the hydrophobic carbon paper occurs. In both cases, the final current density is around 125 mA/cm^2. Although, both characteristics are similar and an improvement of performance cannot be verified for the hydrophobic diffusion layer, the water transport differs significantly. The photos of the water formation in a PEMFC with a hydrophobic carbon paper in Fig. 14 can be compared with the photos 1–5 in Section 4.1 describing the water buildup in a fuel cell with standard TGP-H-090. Hereby, the air volume flows differ but the characteristically formation of water droplets in case of a hydrophobic carbon paper can also be observed for an air-flow of 150 ml/min.

In case of a hydrophobic carbon paper, the water appears not primarily near the air inlet but randomly distributed, see photo 6. The water produced at the cathode can hardly penetrate the carbon paper. The hydrophobic character seems to act like a barrier for the liquid. Only, where the water pressure is high enough, small droplets can permeate through close gaps of the diffusion layer to get visible in the channel. As photo 7 shows, these droplets swell due to more and more product water. Furthermore, the droplets formed are able to move due to kinetic energy of the air-flow and the decreased surface tension of the hydrophobic papers. Agglomeration follows and even in case of a hydrophobic diffusion layer the water buildup can lead to a totally blocked channel (photo 8), which can cause enormous performance losses. The outlet temperature and humidity of air are almost the same during operation with standard and hydrophobic carbon papers. While the outlet humidity increases sharply to a value of more than 100% RH, the outlet temperature stabilizes at 27 °C.

In case of the hydrophilic diffusion layers a moderate decrease of current density can be presented. One reason for higher current densities than in case of standard and hydrophobized carbon papers is seen in the water absorbing effect of the hydrophilized backing layers. Due to the widely distribution of product water the water content of the MEA, which is in direct contact to the wet carbon papers, is homogenized. Cell performance that is heavily dependent on water content of the MEA can be improved. In further run of current density, a second slump cannot be observed. The curve stabilizes on a current density level of 220 mA/cm^2 after 40 min. Due to an increased current density of more than 75% compared to the final current densities of a fuel cell with standard or hydrophobized carbon papers, the outlet temperature is fractionally higher. It is measured to be 29 °C. Although, the air outlet humidity increases up to 100% RH, a total clogging of the air channels can be avoided. The backing layers while acting as a sponge minimize even the formation of discrete droplets. The photos of the air channels taken during operation look similar to photo 1 presented in Fig. 5. Hereby, the same investigations are made for TORAY® carbon papers of 170 μm (TGP-H-060) thickness.

In fact, the effective porosity of the diffusion layer is reduced due to absorbed product water but at the same time the product water is recovered from the cathode catalyst surface. A water barrier between cathode and diffusion layer as assumed in case of the hydrophobic carbon paper is prevented. Reduced gas diffusion inside the diffusion layer seems to be less interactive than inside the cathode catalyst layer. This effect can be ascribed to different pore-sizes of the catalyst and diffusion layer, respectively, and the amount of water to flood them. In case of ultra-thin catalyst layers that are composed of nanoparticles, the required water would be enormously lower than in case of carbon papers with macro-pores with a pore diameter of about 40 μm [31].

Once the pores of the backing layers are filled with water, a drop in current density and water accumulation in the gas channels should be observed. Regrettably, we are unable to perform longer measurements with stable hydrophilic conditions of the carbon papers because the hydrophilic effect

degrades. Current densities of reproduced measurements went down uniformly until the same performance is reached as for standard carbon papers. This effect is ascribed to a deterioration of the hydrophilic character due to a washing out of the water-soluble tenside. Investigations of the contact angle of hydrophilic carbon papers that were inserted for 5 min in an ultrasonic bath showed similar results than presented for a standard TGP-H-060 in Fig. 12a. Another negative impact could be that cations (Na^+) emerged from sodium dodecyl sulfate enter the polymer electrolyte membrane where they displace H^+ ions and decrease its conductivity [38]. Both effects could also be a reason for the decrease in current density shown in Fig. 13.

Opposite to conventional PEM fuel cells that are operated at temperatures around 70 °C, here, measurements of a transparent fuel cell operated at 30 °C and ambient pressure are presented. It has shown that hydrophilic coating of the backing layers can prevent total clogging of air channels due to accumulated product water. However, it has to be pointed out that the choice of diffusion layer characteristic is strongly dependent on operating temperature and that our results cannot directly be converted to higher operating conditions. But during cold-start and outdoor operation of PEM fuel cells temperatures of less than 30 °C are likely be valid [39]. At least in such cases, hydrophilized backing layers can enhance the fuel cell performance. In future, hydrophilic materials or alternative coating technologies to hydrophilize diffusion layers permanently have to be investigated and tested under different operating conditions. Another technical application of hydrophilic or partial hydrophilic diffusion layers could be the transport of water from wet areas to dry areas or into water reservoirs.

5. Conclusions

As shown, water management is one of the critical issues to be solved in the design and operation of PEM fuel cells. Especially, in case of small fuel cells operated at room temperature water flooding may appear. As presented in this paper, even totally clogged flow channels are possible that result in enormous performance losses. The results obtained clarify the necessity of proper control of water content inside an operating fuel cell. Active, e.g. air-flow regulation, and passive, e.g. diffusion layer characteristics, mechanisms are investigated. Thereby, results of two analytical models are in good agreement with the operation at different air-flow rates. If active control of the water management can not be guaranteed due to size and power demand of auxiliary equipment, passive possibilities of intervention are required. One alternative is to manipulate the characteristic of the used diffusion or backing layers. It has shown that the use of standard, hydrophobized and hydrophilized carbon papers directly influence the accumulation of product water in the gas channels of a transparent cathode. In case of operating temperatures of around 30 °C as they can occur during startup and outdoor operation, a hydrophilization of diffusion layers turned out to be very effective in respect of fuel cell performance. Next to the profit for selecting material and operating conditions, the optical visualization of internal water transport phenomena can be used as a basis for modeling liquid water transport in PEM fuel cells.

References

[1] C.K. Dyer, J. Power Sources 106 (2002) 31–34.
[2] C. Hebling, et al., Fuel cells for low power applications: construction, simulation and measurement, in: Proceedings of HYFORUM 2000, vol. II, München, Germany.
[3] F.N. Büchli, S. Srinivasan, J. Electrochem. Soc. 144 (8) (1997) 2767–2772.
[4] K.-H. Choi, et al., J. Power Sources 86 (2000) 197–201.
[5] G.J.M. Janssen, M.L.J. Overvelde, J. Power Sources 101 (2001) 117–125.
[6] D.R. Sena, et al., J. Electroanal. Chem. 477 (1999) 164–170.
[7] T.A. Zawodzinski, et al., J. Electrochem. Soc. 140 (4) (1993) 1041–1047.
[8] Z.H. Wang, C.Y. Wang, K.S. Chen, J. Power Sources 94 (2001) 40–50.
[9] J.J. Baschuk, X. Li, J. Power Sources 86 (2000) 181–196.
[10] D.M. Bernardi, M.W. Verbrugge, J. Electrochem. Soc. 139 (9) (1992) 2477–2491.
[11] N. Djilali, D. Lu, Int. J. Therm. Sci. 41 (2002) 29–40.
[12] I.-M. Hsing, P. Futerko, Chem. Eng. Sci. 55 (2000) 4209–4218.
[13] G. Maggio, V. Recupero, L. Pino, J. Power Sources 101 (2001) 275–286.
[14] T.V. Nguyen, R.E. White, J. Electrochem. Soc. 140 (8) (1993) 2178–2186.
[15] T. Okada, G. Xie, M. Meeg, Electrochim. Acta 43 (14-15) (1998) 2141–2155.
[16] T.E. Springer, T.A. Zawodzinski, S. Gottesfeld, J. Electrochem. Soc. 138 (8) (1991) 2334–2342.
[17] J.S. Yi, T.V. Nguyen, J. Electrochem. Soc. 145 (4) (1998) 1149–1159.
[18] L. You, H. Liu, Int. J. Heat Mass Transfer 45 (2002) 2277–2287.
[19] W.L. Gore and associates GmbH, Technical information on PRIMEA® Power Assemblies, 2000.
[20] M.S. Wilson, C. Zawodzinski, S. Gottesfeld, Direct liquid water hydration of fuel cell membranes, in: Proceedings of the Second International Symposium on Proton Conducting Membrane Fuel Cells, vol. II, Pennington, USA, 1998.
[21] D.L. Wood, J.S. Yi, T.V. Nguyen, Electrochim. Acta 43 (24) (1998) 3795–3809.
[22] T.A. Zawodzinski, et al., Electrochim. Acta 40 (3) (1995) 297–302.
[23] K. Ledjeff-Hey, Brennstoffzellen, Practical Course, Gerhard Mercator University Duisburg, Germany, 1998.
[24] P. Argyropoulos, K. Scott, W.M. Taama, Electrochim. Acta 44 (1999) 3575–3584.
[25] J. Ihonen, et al., Electrochim. Acta 46 (2001) 2899–2911.
[26] T.E. Springer, M.S. Wilson, S. Gottesfeld, J. Electrochem. Soc. 140 (12) (1993) 3513–3526.
[27] J. Larminie, A. Dicks, Fuel Cell Systems Explained, Wiley, West Sussex, England, 2000, pp. 69–81, ISBN: 0 471 49026 1.
[28] K. Lucas, Thermodynamik, Springer, Berlin, Germany, 1995, pp. 73–90, ISBN: 3 540 58925 2.
[29] VDI-Wärmeatlas, 5, Auflage, VDI-Verlag GmbH, Düsseldorf, Germany 1998, Da 32-Da 34.
[30] A. Rowe, Y. Li, J. Power Sources 102 (2001) 82–96.

[31] Toray Deutschland GmbH, Technical information on TGP-H Carbon Papers, 2001.
[32] D. Bevers, R. Rogers, M. von Bradke, J. Power Sources 63 (1996) 193–201.
[33] V.A. Paganin, E.A. Ticianelli, E.R. Gonzalez, J. Appl. Electrochem. 26 (1996) 297–304.
[34] Z. Qi, A. Kaufman, J. Power Sources 109 (2002) 38–46.
[35] L. Giorgi, et al., Electrochim. Acta 43 (24) (1998) 3675–3680.
[36] L.R. Jordan, et al., J. Power Sources 86 (2000) 250–254.
[37] C.S. Kong, et al., J. Power Sources 108 (2002) 185–191.
[38] J. St-Pierre, et al., J. New Mater. Electrochem. Syst. 3 (2000) 99–106.
[39] D. Chu, et al., J. Power Sources 96 (2001) 174–178.